Article

Calculating Energy and Its Spatial Distribution for a Subsurface Urban Heat Island Using a GIS-Approach

Julian A. V. Schweighofer *, Michael Wehrl, Sebastian Baumgärtel and Joachim Rohn

GeoZentrum Nordbayern, Department Geographie und Geowissenschaften, Friedrich-Alexander-University Erlangen-Nuremberg (FAU), Schlossgarten 5, 91054 Erlangen, Germany; michael.wehrl@fau.de (M.W.); sebastian.baumgaertel@fau.de (S.B.); joachim.rohn@fau.de (J.R.)
* Correspondence: julian.schweighofer@fau.de

Abstract: In urban areas, the human influence on the city-ecosystem often results in a Subsurface Urban Heat Island (SUHI), which can be used geothermally. Unfortunately, a model of a SUHI does not consider the geology and hydrogeology of the subsoil. These can vary significantly over short distances, and are of considerable importance for the energy balance. In this work, we calculated the energy and its density stored in the subsoil via a SUHI. For this so-called energy-SUHI (e-SUHI), we evaluated the geology and its physical parameters for the first 20 m below ground level in the German city of Nuremberg and linked them to measured underground temperatures in a GIS application. This approach revealed stored energy of 1.634×10^{10} MJ within the soil and water for the study area with an area of 163 km^2 and a volume of 3.26×10^9 m^3. It corresponds to an average energy density of 5.0 MJ/m^3. The highest energy density of 16.5 MJ/m^3 was found in the city center area and correlated well to increases in subsurface temperature. As expected, our model reacts sensitively to thickness changes in the geological layers and the unsaturated zone.

Keywords: Subsurface Urban Heat Island (SUHI); energy-SUHI; GIS; geothermal energy

1. Introduction

Urban environments shape the thermal regime of their surroundings on various levels. They create an urban climate, which often results in positive temperature anomalies in the atmosphere as an Urban Heat Island UHI [1–3]. A similar effect can be observed underground. This is known as a Subsurface Urban Heat Island (SUHI), when soil- and groundwater temperatures are higher than in the surrounding area due to anthropogenic influences. For some cities such as Munich, Paris, Winnipeg, Cardiff, and Osaka, spatio-temporal spreads of the SUHI are already well documented. They show positive temperature anomalies in the subsurface up to several Kelvin [3–11]. Main causes for the warming include soil surface sealing, heat input through surfaces and buildings, as well as infiltration of heated rain and wastewater [12–16]. Simultaneously, proportions of vegetation and water surfaces decrease and thus further reduce cooling effects caused by evapotranspiration. This results in further heating of land surface and soil temperatures [17–21]. In addition, part of the recent rise in groundwater temperatures can be attributed to global warming [22,23].

Various studies report that the anthropogenic warming of soils has profound influences on ecosystems and influences biological, chemical, and physical processes [24–27]. One possible consequence includes increased concentration of dissolved ions, which can worsen drinking water quality [28]. To minimize the negative influences on ecological systems and associated groundwater quality, a geothermal use of urban heat energy is recommended [29]. In addition to the classic geothermal systems such as borehole heat exchangers or energy baskets, numerous alternative approaches exist for thermal energy use. For example, tunnel constructions can include tunnel wall heat exchangers. With these structures' waste heat from vehicles such as subways can be used for energy generation

to help minimizing heating of the underground [30,31]. Other solutions deal with the direct use of groundwater for heating infrastructures [32]. For instance, in Nuremberg, it was discussed how groundwater could serve to keep bridge elements and motorway ramps free of snow and ice. Field tests have shown that this can be expected to de-ice road surfaces with ambient temperatures as low as $-10\ °C$ [33].

Although the SUHI is a well-researched phenomenon and is used as a basis for the site assessment of geothermal systems, only a small part of the previous work deal with thermal performance and energy potential of urban areas [34–37]. In such studies, the total energy of a SUHI was calculated from the heat capacity of the heated material and the temperature anomaly. For the cities Winnipeg and Cologne, this analysis was conducted [34]. This study showed that this energy demand would be able to cover the heating demands for 2.3 and 10.7 years for Winnipeg and Cologne, respectively. However, even in these studies, no investigation of the spatial distribution of the energy and energy density was carried out. In a new approach, this work therefore aims to develop the SUHI of the city of Nuremberg with parameters from hydrology and geology in a GIS application to a so-called Energy-Subsurface Urban Heat Island (e-SUHI). The e-SUHI is a high-resolution map of the energy density distribution in the first 20 m below ground level. The energy density better describes the technical potential of a SUHI for geothermal by identification of the e-SUHI locations with a high energy density. Furthermore, locations with similar temperature conditions can be distinguished by their energy density. In the following, we present new data and the methodologies for determinations of an e-SUHI in the city of Nuremberg. This urban environment is highly suitable for this approach because of its subsurface with highly variable soil and aquifer thicknesses and layers, and a wealth of data for geothermal energy use.

2. Materials and Methods

The German city of Nuremberg is located at latitude $49°27'$ N longitude $11°5'$ E in the State of Bavaria in a flat-hilly region of the South German Scarplands at an altitude of 284–408 m above sea level. The Rhine-Main-Danube Canal, as well as the rivers Pegnitz and Rednitz, flow through the city. The city has an area of 186 km^2 with 518,000 inhabitants. In the north, east, and south, Nuremberg borders on forest areas, while in the west, it connects seamlessly to the city of Fürth. The 163 km^2 large study area covers the urban center, suburbs, and a large rural area in the north that servers as agricultural land. Nuremberg's climate belongs after Köppen-Geiger classification to the warmly moderate rain climate (Cfb) with an annual average temperature of around 9.3 °C and annual precipitation of approximately 630 mm/a [38]. Figure 1 shows the position of Nuremberg within Germany, and the borders of the investigated area.

Nuremberg's underground is composed of continental and marine sedimentary rocks. These Mesozoic sedimentary rocks consist of Triassic sandstones and claystone from the Middle Keuper. They are locally covered by Cenozoic sediments with varying thicknesses of up to 30 m. The sediments include fluviatile sands, gravels, and boulders, alluvial clays, silt, sands, and gravels, as well as aeolian sands. The thickest sedimentary cover exists within the former river valleys of the rivers Pegnitz and Rednitz [39,40]. For our GIS application, we further assume a simplified geological model, which distinguishes between Mesozoic sandstones and Cenozoic sands. Several aquifers exist below Nuremberg, although only the uppermost aquifer with its Mesozoic sedimentary rocks and Cenozoic sediments is used for geothermal purposes. Deeper aquifers may not be drilled due to water law restrictions.

A detailed workflow for determining the e-SUHI is provided in Figure 2. In order to calculate the energy and energy density of the e-SUHI, knowledge of temperature anomalies and the material constants of the rocks is necessary. Therefore, we first determined the thickness of the unsaturated zone and the different geological layers, the porosity and specific heat capacity of the rocks, and the groundwater temperatures. Then, location-dependent data are imported into a GIS application and an interpolation method is used

to generate raster files for each layer. In a final step, these grid files are used to calculate the mean energy density in [MJ/m^3] of the first 20 m below ground level (b.g.l.). This outlines temperature anomalies. In the following, we describe the individual parameters' determination and the calculation of the energy and the energy density.
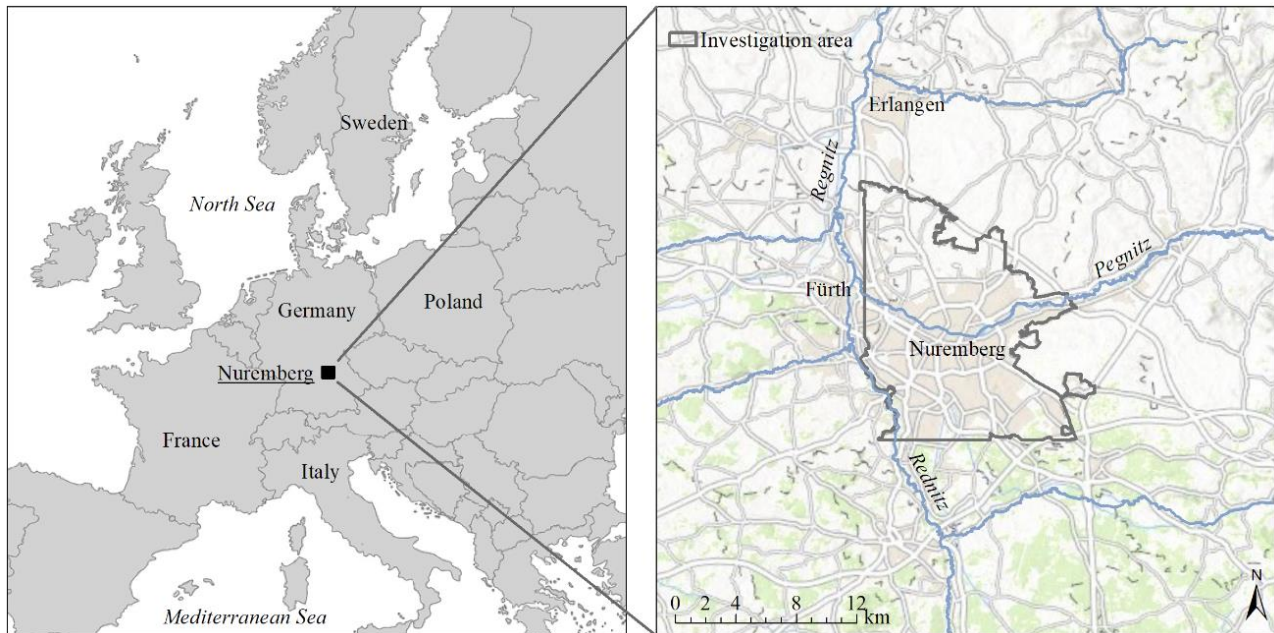

Figure 1. Location of Nuremberg in Europe and Germany. The map on the right hand shows the outline of the investigated area. Sources: Esri, HERE, DeLorme, increment P Corp., NPS, NRCan, Ordnance Survey, © OpenStreetMap contributors, USGS, NGA, NASA, CGIAR, N Robinson, NCEAS, NLS, OS, NMA, Geodatastyrelsen, Rijkswaterstaat, GSA, Geoland, FEMA, Intermap and the GIS user community.
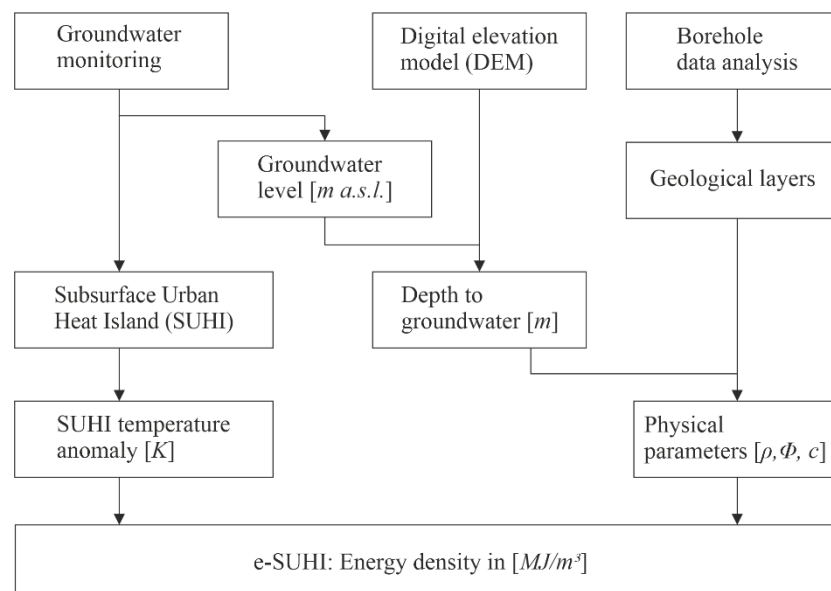

Figure 2. Workflow for the calculation of an energy-Subsurface Urban Heat Island (e-SUHI). The energy density in the subsurface caused by the SUHI is determined by temperature anomalies of the SUHI and physical rock parameters. We assume a subsurface temperature anomaly when the annual mean groundwater temperatures exceed 10.5 °C.

As a data basis, we used geological stratigraphic inventories from the Bavarian State Office for the Environment, groundwater data from the Nuremberg Environmental Office and from own groundwater monitoring, as well a digital elevation model (DEM-2) from the Bavarian Agency for Digitisation, High-Speed Internet and Surveying, as shown in Figure 3. Locations of wells are shown in Figure 4. Data sets consisted of 4309 geological profiles, 972 groundwater level measurements, and over 400 temperature profiles. These data are available after consulting the authors and the responsible authorities. The type of data collection and evaluation is described in more detail below.
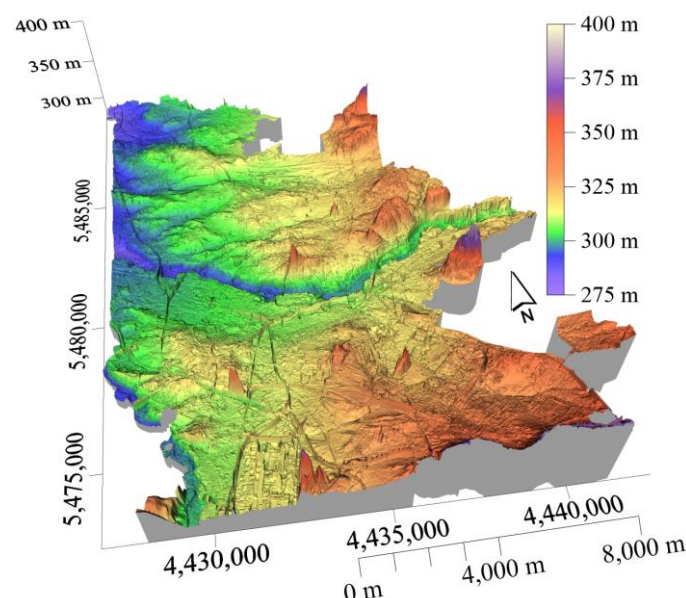

Figure 3. 3D rendering of a digital elevation model (DEM-2) of the Nuremberg investigation area from an airborne laser scan. The spatial resolution is 2 m, while the height accuracy is better than ±0.2 m. The raster file of the DEM-2 is needed to calculate the thickness of the unsaturated zone. Data source: Geobasisdaten © Bavarian Agency for Digitisation, High-Speed Internet and Surveying, 2012.

For the description of the SUHI, we collected an extensive database of groundwater temperatures from 418 groundwater measuring points. The data collection was carried out with a temperature, level, and conductivity (TLC) meter with an accuracy of <0.1 K. In addition, 30 data loggers were evaluated. These recorded groundwater temperatures twice a day at a constant depth. The data cover a time span from 2015 to 2020. For an accurate description of the SUHI, influences of seasonal fluctuations of soil temperatures and convection-conditioned heat transport within a groundwater measuring point should be kept as low as possible [41]. For this purpose, we recorded a vertical temperature depth profile for each groundwater measuring point in 1-m-steps, starting from ground level. For the description of the SUHI, we only used the temperature value, which was recorded at the deepest point in the groundwater well. An additional boundary condition excluded temperature values above 5 m or below 20 m. If several temperature profiles from different months were available for the groundwater measuring point, we calculated the mean temperature. From these temperature values, we created an isothermal map for the Nuremberg groundwater temperature as shown in Figure 5A. However, because we need the underground temperature anomaly in Kelvin as an input parameter for the e-SUHI, we also needed a defined value for natural underground temperatures. This defined value is based on groundwater temperatures underneath meadows and in forests around Nuremberg. Here groundwater temperatures range between 8.5 and 10.5 °C. Because of this observation, we have decided to consider a SUHI-effect ΔT in Kelvin when annual mean groundwater temperatures T_m exceeded $T_0 = 10.5$ °C, shown in Equation (1).
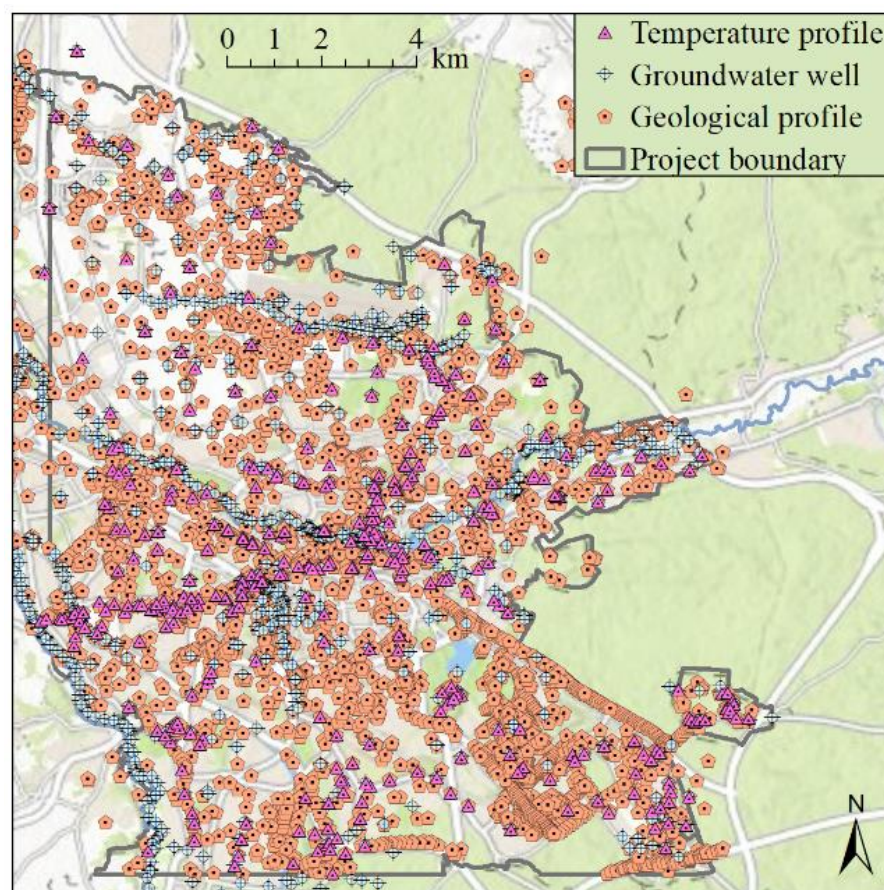
$$\Delta T = T_m - T_0 \tag{1}$$

Figure 4. Spatial distribution of the boreholes and wells with for temperature profiles, the distance to groundwater, and the geological model, Sources: Esri, HERE, DeLorme, increment P Corp., NPS, NRCan, Ordnance Survey, © OpenStreetMap contributors, USGS, NGA, NASA, CGIAR, N Robinson, NCEAS, NLS, OS, NMA, Geodatastyrelsen, Rijkswaterstaat, GSA, Geoland, FEMA, Intermap and the GIS user community.

Because the volume-related specific heat capacity of rock depends on the degree of water saturation of the underground, the thickness of the unsaturated zone was determined for the whole study area. Data were collected from a measurement campaign in 2016 with almost 1000 individual values of groundwater levels and auxiliary points along surface waters. At the groundwater wells, the groundwater level was recorded with a cable light plummet or data logger. From these measured values, we created a groundwater contour map. In a next step, this map was merged with the ground level heights from a digital elevation model (DEM) with a spatial resolution of 2 m in a GIS application in order to generate a comprehensive map of the thickness of the unsaturated zone. This is shown in Figure 5B.

A description of the geology is necessary to determine the energy density within the first 20 m b.g.l. We assume two different geological units with Quaternary loose sediments and Triassic sandstone. From a database of about 4000 drill cores, we created two grid files for the thickness of the Triassic sandstone and the Quaternary loose sediments, where the thickness of the Quaternary loose sediments is shown in Figure 5C. We intersected these two geological layers with the thickness of the unsaturated zone to produce four grid files representing the thickness of dry and water-saturated Quaternary loose sediments and dry and water-saturated sandstones. In the next step, we calculated the thermal energy Q_{1-4} stored in each of these four (hydro-) geological layers, according to Equation (2), taking into account their different physical parameters after Table 1. This gave us four individual raster files on the stored energy in the subsurface from 0–20 m. Additionally, taking into

account the thickness of the four (hydro-) geological layers and their associated specific heat capacities, a raster file was created that shows the average specific heat capacity of the subsurface for the first 0–20 m, shown in Figure 5D.
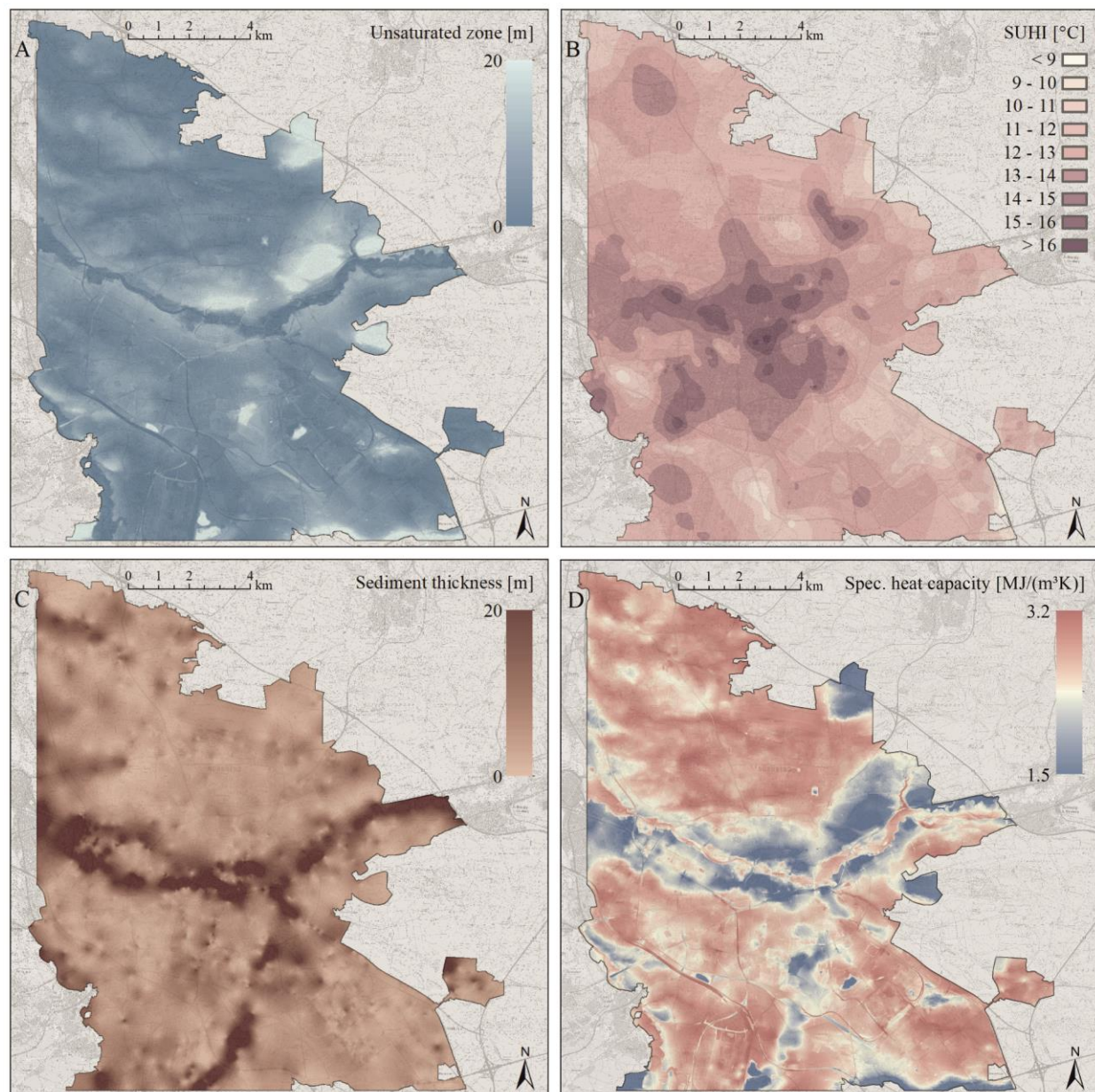

Figure 5. Raster files calculated with GIS about the spatial distribution of (**A**) the thickness of the unsaturated zone in [m], (**B**) the measured groundwater temperatures in [°C]—the SUHI is clearly visible within the city center, (**C**) the thickness of the Quaternary sediments in [m], and (**D**) the mean specific heat capacity in [MJ/(m^{3}K)] for the first 0–20 m b.g.l. Sources: (**A**,**B**): Own Measurements and data from Environmental Agency of Nuremberg. (**C**): Data from Bavarian State Office for the Environment, LfU, www-lfu.bayern.de. (**A**–**D**): Topographic basemap, TK 1:25 000, ATKIS $^®$, DLM1000; Copyright © Bundesamt für Kartographie und Geodäsie, 2008.

Table 1 shows the rock parameters of the Nuremberg subsurface, while we only used the porosity and the volume-related specific heat capacity to calculate the energy density. The material properties of sand were used for the description of the Quaternary loose sediments, those of sandstone for the Triassic sandstones. The highest specific heat capacity for water-saturated sandstone in the investigation area is 3.2 MJ/(m^{3}K). The lowest specific heat capacity is dry sand with 1.5 MJ/(m^{3}K), 47% of the specific heat capacity of water-

saturated sandstone. The porosity only depends on the sediment type and ranges between 0.25 for sandstone and 0.35 for sand.

Table 1. Rock parameters, derived from literature data for modelling the e-SUHI.

Material	Bulk Density ρ_{bulk} [10^3 kg/m^3]	Porosity φ [-]	Weight-Related Specific Heat Capacity c_p [J/kg*K]	Volume-Related Specific Heat Capacity $\rho * c_p$ [MJ/(m^{3}K)]
Sand$_{dry}$	1.8–2.2 [c]	0.35 [a]	[-]	1.5 [c]
Sand$_{water-saturated}$	1.9–2.3 [c]	0.35 [a]	[-]	2.5 [c]
Sandstone$_{dry}$	2.0–2.3 [b]	0.25 [a]	951–1017 [b]	2.2 [c]
Sandstone$_{water-saturated}$	[-]	0.25 [a]	[-]	3.2 [d]
Water	0.999 [c]	[-]	[-]	4.15 [c]

[a] Values after [42]; [b] values after [43]; [c] values after [44]; [d] value calculated with values from [a] porosity and [c] volume-related specific heat capacity.

Using the temperature anomaly, the volumes and the specific heat capacities, four individual raster files Q_{1-4} of the stored heat energy, each related to a specific (hydro-)geological layer, are calculated after Equation (2) [34,36].

$$Q_{1-4} = Q_s + Q_w = V * \rho * c_p * \Delta T + V * n * \rho * c_p * \Delta T \tag{2}$$

where Q_{1-4} is the thermal energy in [MJ] for each (hydro-)geological layer, Q_w and Q_s are the individual amounts of energy stored in water (Q_w) and soil (Q_s). V describes the volume of the investigated reservoir in [m^3], n is the rock porosity in [-] $\rho * c_p$ is the material constant of the volume-related specific heat capacity of soil and water, and ΔT is the temperature anomaly in [K], caused by the SUHI-effect as described in Equation (1). The sum of these four individual raster layers Q_{1-4} equals the total stored heat energy Q for the whole city of Nuremberg with a resolution of $1 \times 1 \times 20$ m^3.

By dividing the grid file of the total thermal energy Q by the volume, the energy density w in [MJ/m^3] is obtained, as shown in Equation (3).

$$w = \frac{Q}{V} \tag{3}$$

where w is the energy density in [MJ/m^3], V describes the body volume for which the energy was calculated, and Q is the energy excess of the first 20 m below ground level.

3. Results

Figure 5A shows that the values of the unsaturated zone vary between 0 and >20 m over the entire investigated geological body for the city of Nuremberg. The average distance between the ground water level and the ground surface is 5.9 m. Larger distances of more than 10 m were frequently found within the city center and in elevated areas. Low values occurred particularly in the outskirts of the city, agriculturally used areas, alluvial zones, and forests.

The groundwater temperatures in Figure 5B show high spatial variabilities and range between 8.5 and 17.0 °C. The temperatures of the SUHI are comparable with those of other German cities with temperature peaks between 13 and 18 °C [9]. A general increase in temperature from wooded areas to bare soil and suburbs to the city center is obvious. Temperature increases of 2–3 K could already be measured between forest and farmland. This is most likely due to the different land use and the resulting absence of natural cooling processes by evapotranspiration and photosynthesis activity [45]. In our study, fallow land, bare soil, and farmland reach temperatures between 11–13 °C. Likewise, we could observe that smaller villages can also develop underground temperatures of approximately 13 °C. This shows that the phenomenon of the suburban heat island cannot be reduced to the

city's effect alone. This phenomenon can be observed in Figure 5C in the northern part of our study area. Within the urban area, underground temperatures between 13 and 15 °C are most commonly found. Locally, hotspots of up to 17 °C are possible that result from waste heat from underground infrastructures. Colder spots within the urban area reach values of 10 to 11 °C and are limited to meadows, parks, and areas close to water.

The thickness of the Quaternary loose sediments in Figure 5C ranges between 0 and >20 m, with the thickest layers found in the Quaternary sediment-filled glacial valleys. Small-scale anthropogenic fillings are mainly found in the urban area. The north of Nuremberg has extensive quaternary sediment covers of 0–4 m. The mean specific heat capacity derived from the (hydro)-geological 4-layer-case, within the first 0–20 m of the subsurface in Figure 5D, varies from 1.5 MJ/m^{3}K for dry sand to 3.2 MJ/m^{3}K for water-saturated sandstone. With this, the average specific heat capacity of the entire investigation area for the first 0–20 m b.g.l. is 2.8 MJ/m^{3}K. This value is higher than the specific heat capacities of dry and water-saturated sands and dry sandstones. Only the water-saturated sandstone with 3.2 MJ/m^{3}K has a higher specific heat capacity.

The e-SUHI in Figure 6 shows the spatial distribution of the mean energy density of the subsurface in MJ/m^3. Additionally, the SUHI is displayed as an isothermal map for better comparison with the e-SUHI. The hotspots of the e-SUHI are similar to the SUHI in the city center. Additionally, isolated peaks with high energy densities of up to 8 MJ/m^3 at about 13 °C can be detected in the outskirts and the surrounding villages. Energy densities of 2–6 MJ/m^3 at 11–13 °C are expected in the north, which is strongly influenced by agricultural land use. The highest energy density of 16.5 MJ/m^3 at 16 °C and a specific heat capacity of 3 MJ/m^{3}K were evident in the city center.

With a specific heat capacity of 3.2 MJ/(m^{3}K) and a thermal anomaly of up to 6.6 K/17.1 °C, an energy density of up to 21.2 MJ/m^3 is theoretically possible. Thus, due to the geological and hydrogeological properties, a maximum of 78% of the technically possible energy density was achieved. Note that the e-SUHI does not show a continuous increase from the outskirts to the city center. Instead, individual energy hotspots are distributed over the entire city area, where they are almost identically pronounced. For the whole study area, the mean energy density was 5.04 MJ/m^3 with a temperature anomaly of 1.8 K (12.3 °C) and a specific heat capacity of 2.8 MJ/(m^{3}K). We placed a profile through the working area in N-S orientation in order to create a profile section through the e-SUHI. This cross section is shown in Figure 6, and the plots of the extracted parameters are shown in Figures 7–9.

The plotted points are located exclusively within the two straight lines of the lower and upper technical boundary resulting from the minimum (1.5 MJ/m^{3}K) and maximum (3.2 MJ/m^{3}K) possible specific heat capacity of the rock and the measured temperature anomaly. Different energy densities at the same temperature are due to the different heat capacities of the geological layers. Thus, the energy densities can differ at the same temperature by a factor of 2.1. On average, the points plot closer to the upper technical boundary. The lower technical boundary cannot be reached by the measuring points due to the fact that we were unable to measure the groundwater temperature when the groundwater level fell below 20 m b.g.l. However, a thickness of the unsaturated zone of more than 20 m is a prerequisite for an average specific heat capacity of 1.5 MJ/m^{3}K. This particular case cannot be shown directly in Figure 10. They are however evident as interpolated values in Figure 5D. The determined average values for the Nuremberg investigation area are 5.0 MJ/m^3 for the energy density and 12.3 °C for the groundwater temperature are shown in Figure 10 as a yellow star. Further parameters determined for the entire Nuremberg city area are shown in Table 2.
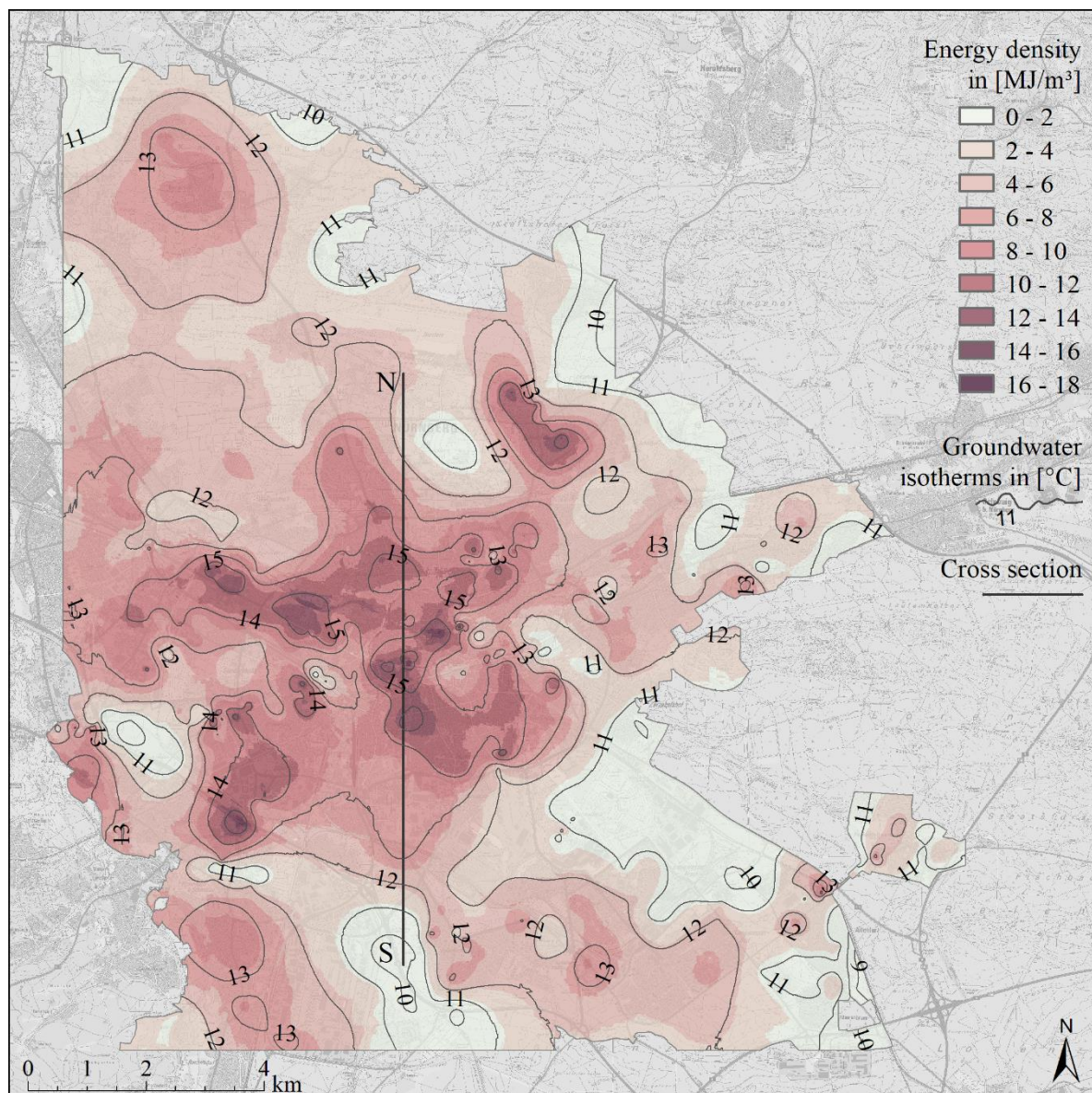
Figure 6. Spatial distribution of the energy density and suburban heat island of the city of Nuremberg. Topographic basemap, TK 1:25 000, ATKIS ®, DLM1000; Copyright © Bundesamt für Kartographie und Geodäsie, 2008.
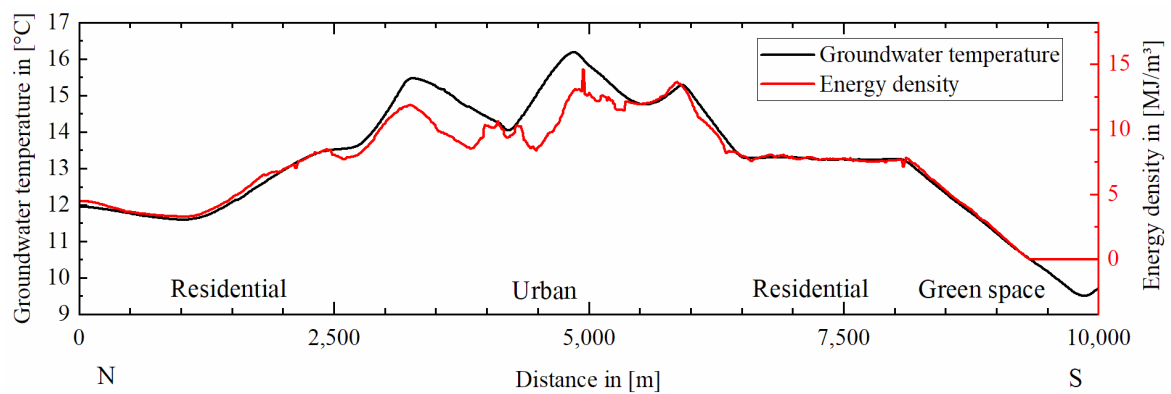

Figure 7. Cross-section in the N-S direction through the Nuremberg working area. The extracted data show the groundwater temperature of the SUHI and the energy density of the e-SUHI.
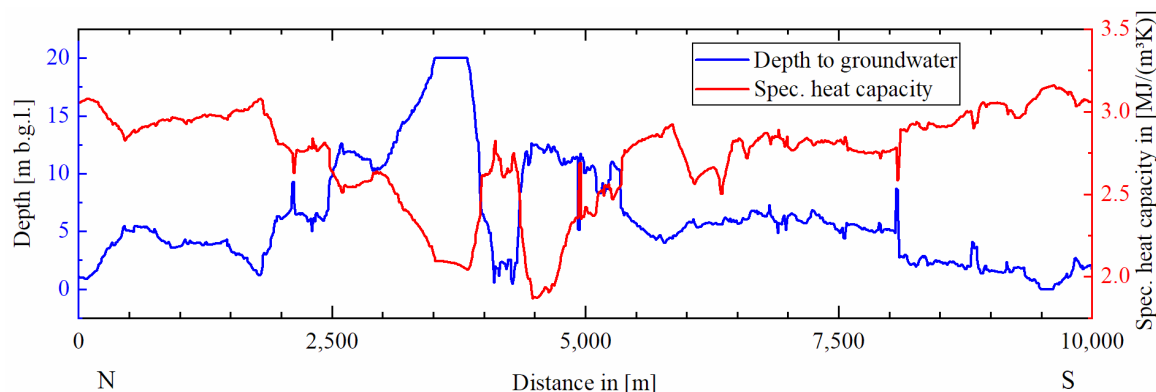
Figure 8. Cross-section for the unsaturated zone and the specific heat capacity of the underground. The parameters show a negative correlation.
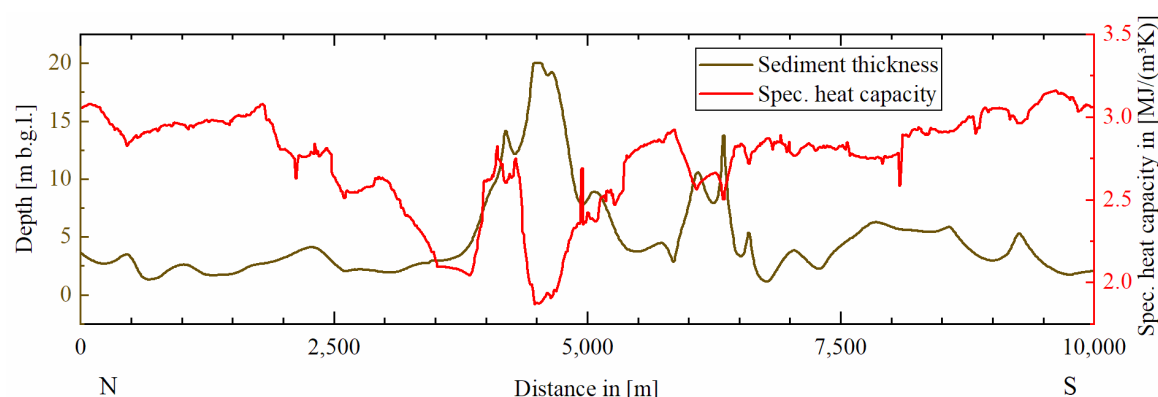

Figure 9. Cross-section for the sediment thickness and the specific heat capacity. In comparison to the unsaturated zone, only an unclear correlation between sediment thickness and specific heat capacity can be seen.

Figure 7 shows the groundwater temperatures of the SUHI and the energy density of the e-SUHI as a cross-section through the urban heat island. Additionally, in the cross-section, it is visible that the SUHI and e-SUHI increase towards the city center. The peaks of the two lines are almost identical. The energy density in suburbs and settlement areas is limited to about 8 MJ/m^3. However, within the city center it increases to up to 16 MJ/m^3. On green areas, it decreases to 0 MJ/m^3 as soon as the groundwater temperatures fall below 10.5 °C. The most significant deviations of the curves of temperature and energy density are found within 3000 to 5000 m within the urban city center. The energy density is underrepresented when compared to the temperature. The energy density is a result of the temperature and the specific heat capacity. If the specific heat capacity in Figure 8 falls below its average value of 2.8 MJ/m^3/K, the energy density curve in Figure 7 falls below the curve of the groundwater temperature as a consequence. Figures 8 and 9 show the dependence of the specific heat capacity on the groundwater level and sediment thickness. At 3000–5000 m a large thickness of the unsaturated zone results in low heat capacities in Figure 8 and the further in the low energy density in Figure 7. The negative influence of the Quaternary loose sediments on the energy density is obvious at 6000–6500 m in Figure 9. Here, an increase in the sediment thickness is accompanied by a decrease in specific heat capacity and energy density. For all groundwater observation wells, the groundwater temperature was plotted against the mean energy density and is shown in Figure 10.

The highest value of the energy density is 16.5 MJ/m^3 at 16.0 °C while the highest measured temperature is 17.1 °C at an energy density of 16.1 MJ/m^3. The total energy excess stored in the first 20 m b.g.l. is 1.634×10^{10} MJ. This energy amount corresponds to the energy produced if a power plant with an installed capacity of 1 GW would run continuously for half a year.
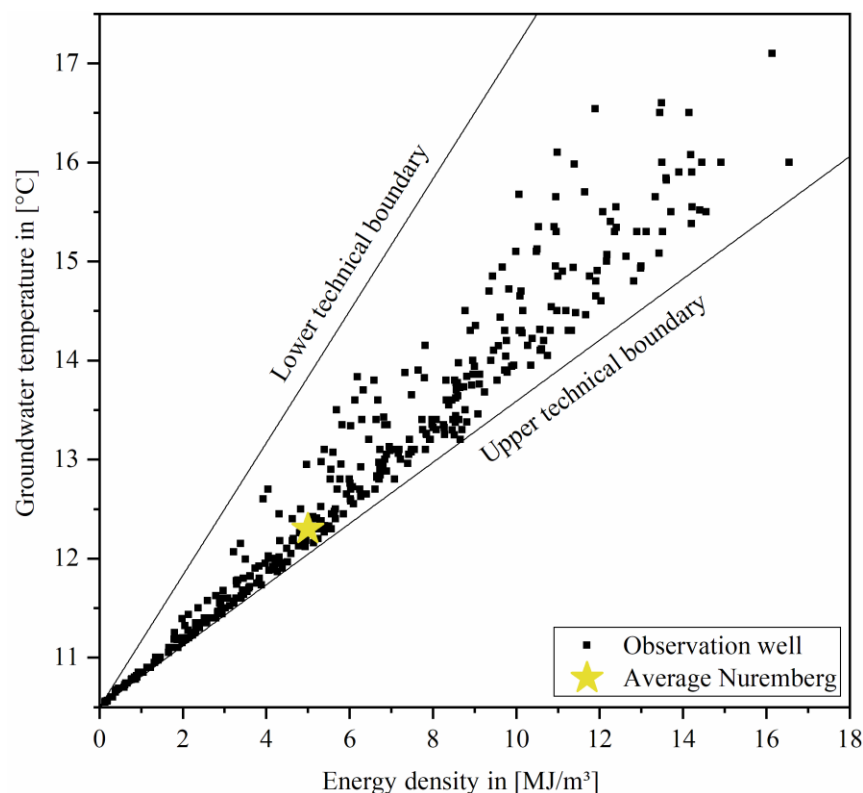
Figure 10. The plot comparing the mean energy density against the groundwater temperatures for all groundwater observation wells.

Table 2. Determined hydrogeological and physical parameters for the Nuremberg study area.

	Depth to Groundwater [m]	Groundwater Temperature [°C]	Sediment Thickness [m]	Specific Heat Capacity [MJ/m³K]	Energy Density [MJ/m³]
Minimum	0.0	8.5	0.0	1.5	0.0
Maximum	20.0	17.1	20.0	3.2	16.5
Mean	5.9	12.3	4.3	2.8	5.0
Standard deviation	4.5	1.1	3.8	0.3	2.9
Stored Energy	1634×10^{10} MJ/16.34 PJ				

4. Discussion

Since the GIS model only distinguishes between four different hydrogeological settings as given in Table 1, there are uncertainties with regard to the specific heat capacity of the subsurface: This is mostly due to more heterogeneity than we were able to consider in our GIS application. A simple geological model was assumed in this application, because the program we use does not allow complex 3D-subsurface-modelling. In addition, heat transport mechanisms and other rock parameters such as thermal conductivity, hydraulic gradient, and permeability of the subsurface, which are relevant for the temperature development within a SUHI, were not considered in this study such as in other studies [46]. It was also not considered that the groundwater level is affected by seasonal fluctuations, and thus the specific heat capacity of our model changes within a year. Over the year, Nuremberg has a balanced groundwater budget, so that we assume negligible variations in the long term [47,48].

For our model, groundwater temperatures were averaged over a year. Seasonal variations are therefore not taken into account, and our averaged model cannot be directly related to a specific date. For the Nuremberg study area, it is also currently unclear whether and how much urban soil and groundwater temperatures will increase in the long

term compared to the surrounding area. We recommend that groundwater temperatures continue to be monitored. Researchers from the neighboring Czechia and Slowenia have already investigated the question of the mean annual warming rate of the soil [22]. They have shown that a mean warming of 0.034 K/a is to be expected at a depth of 38 m. It is interesting to note that soil warming is dependent on global warming and anthropogenic building. For our model, this means that in the long term our natural mean soil and groundwater temperatures must be corrected upwards. In addition, it can be assumed that the temperature anomaly in the subsurface will also change with a change in surface development.

Groundwater temperature is considered the greatest uncertainty factor in calculating the e-SUHI. This is because groundwater temperatures have the lowest data density. The interpolation of the groundwater temperatures between the measuring points results in uncertainties and small-scale temperature fluctuations that cannot be recorded. In rural areas, the coverage of piezometers is comparatively small. This is one reason why particularly in the range of settlements and villages, the soil temperatures are only insufficiently recorded. Other works with investigation areas in German and French cities deal with this problem and solve it with approaches from remote sensing. In such approaches, groundwater temperatures are derived from land surface temperatures (LST) and further parameters from land use [21,49]. Root mean square error (RMSE) values of less than 1 K were achieved for several European cities when comparing measured and calculated groundwater temperatures. This possible derivative of groundwater temperatures from LST-data would be a promising approach for Nuremberg, to increase the accuracy of the SUHI and the e-SUHI.

5. Conclusions

This paper presents a first GIS-based high-resolution energy density map at city level as a so-called e-SUHI. For calculating the e-SUHI, the temperature anomaly in the underground of the city was described and linked to physical parameters. In total, 418 groundwater temperatures, almost 1000 groundwater levels, and almost 4000 drill core data were available to calculate the e-SUHI. The energy was calculated from values of the temperature anomaly of the subsurface and the specific heat capacities of the rocks and loose sediments. The energy density of the e-SUHI could be shown to reach up to 16.5 MJ/m^3 at a temperature anomaly of 5.5 K. The average energy density is 5.0 MJ/m^3.

As expected, the highest energy densities were found in the area of the urban city center. Additionally, we were able to show that villages, suburbs, and residential areas on the outskirts of cities can develop high energy densities. The energy density at similar temperatures fluctuates significantly due to geological and hydrogeological differences. For instance, within the inner city, the energy density is underrepresented compared to the underground temperature. This is mainly due to the higher thickness of the unsaturated zone measured within the city center. The quality of the e-SUHI and the SUHI depends largely on the spatial density and distribution of groundwater measuring points.

More accurate results for the e-SUHI would be obtained with a higher number of soil temperatures and a more precise subdivision of the geological layers. For further studies, we recommend calculating the spatial distribution of the energy density of other cities to verify whether further energy density hotspots can be detected here as well.

Author Contributions: Conceptualization, J.A.V.S.; methodology, J.A.V.S.; software, J.A.V.S.; validation, J.A.V.S., M.W., S.B. and J.R.; formal analysis, M.W., S.B. and J.R.; investigation, J.A.V.S., M.W., S.B.; resources, J.A.V.S.; data curation, J.A.V.S.; writing—original draft preparation, J.A.V.S.; writing—review and editing, J.A.V.S., M.W., S.B. and J.R.; visualization, J.A.V.S.; supervision, J.R.; project administration, J.A.V.S., M.W., J.R. All authors have read and agreed to the published version of the manuscript.

Institutional Review Board Statement: Not applicable.

References

1. Oke, T.R. City size and the urban heat island. *Atmos. Environ.* **1973**, *7*, 769–779. [CrossRef]
2. Kardinal Jusuf, S.; Wong, N.H.; Hagen, E.; Anggoro, R.; Hong, Y. The influence of land use on the urban heat island in Singapore. *Habitat Int.* **2007**, *31*, 232–242. [CrossRef]
3. Huang, S.; Taniguchi, M.; Yamano, M.; Wang, C.-H. Detecting urbanization effects on surface and subsurface thermal environment—A case study of Osaka. *Sci. Total Environ.* **2009**, *407*, 3142–3152. [CrossRef]
4. Ferguson, G.; Woodbury, A. Urban heat island in the subsurface. *Geophys. Res. Lett.* **2007**, *34*. [CrossRef]
5. Taniguchi, M.; Uemura, T.; Jago-on, K. Combined Effects of Urbanization and Global Warming on Subsurface Temperature in Four Asian Cities. *Vadose Zone J.* **2007**, *6*, 591–596. [CrossRef]
6. Kataoka, K.; Matsumoto, F.; Ichinose, T.; Taniguchi, M. Urban warming trends in several large Asian cities over the last 100 years. *Sci. Total Environ.* **2008**, *407*, 3112–3119. [CrossRef] [PubMed]
7. Yamano, M.; Goto, S.; Miyakoshi, A.; Hamamoto, H.; Lubis, R.F.; Monyrath, V.; Taniguchi, M. Reconstruction of the thermal environment evolution in urban areas from underground temperature distribution. *Sci. Total Environ.* **2009**, *407*, 3120–3128. [CrossRef]
8. Turkoglu, N. Analysis of urban effects on soil temperature in Ankara. *Environ. Monit. Assess.* **2010**, *169*, 439–450. [CrossRef]
9. Menberg, K.; Bayer, P.; Zosseder, K.; Rumohr, S.; Blum, P. Subsurface urban heat islands in German cities. *Sci. Total Environ.* **2013**, *442*, 123–133. [CrossRef]
10. Farr, G.; Patton, A.; Boon, D.; Schofield, D.; James, D.; Williams, B. Mapping shallow urban groundwater temperatures, a case study from Cardiff, UK. *Q. J. Eng. Geol. Hydrogeol.* **2017**, *50*. [CrossRef]
11. Tissen, C. Groundwater temperature anomalies in central Europe. *Environ. Res. Lett.* **2019**, *14*, 104012. [CrossRef]
12. Kuttler, W. Stadtklima. *Umweltwiss. Schadst. Forsch.* **2004**, *16*, 187–199. [CrossRef]
13. Ferguson, G.; Woodbury, A. Subsurface heat flow in an urban environment. *J. Geophys. Res.* **2004**, *109*. [CrossRef]
14. Taylor, C.A.; Stefan, H.G. Shallow groundwater temperature response to climate change and urbanization. *J. Hydrol.* **2009**, *375*, 601–612. [CrossRef]
15. Menberg, K.; Blum, P.; Schaffitel, A.; Bayer, P. Long Term Evolution of Anthropogenic Heat Fluxes into a Subsurface Urban Heat Island. *Environ. Sci. Technol.* **2013**, *47*, 9747–9755. [CrossRef]
16. Benz, S.A.; Bayer, P.; Menberg, K.; Jung, S.; Blum, P. Spatial resolution of anthropogenic heat fluxes into urban aquifers. *Sci. Total Environ.* **2015**, *524–525*, 427–439. [CrossRef]
17. Taha, H. Urban climates and heat islands: Albedo, evapotranspiration, and anthropogenic heat. *Energy Build.* **1997**, *25*, 99–103. [CrossRef]
18. Mackey, C.W.; Lee, X.; Smith, R.B. Remotely sensing the cooling effects of city scale efforts to reduce urban heat island. *Build. Environ.* **2012**, *49*, 348–358. [CrossRef]
19. Peng, S.; Piao, S.; Ciais, P.; Friedlingstein, P.; Ottle, C.; Bréon, F.-M.; Nan, H.; Zhou, L.; Myneni, R.B. Surface Urban Heat Island across 419 Global Big Cities. *Environ. Sci. Technol.* **2012**, *46*, 696–703. [CrossRef]
20. Maimaitiyiming, M.; Ghulam, A.; Tiyip, T.; Pla, F.; Latorre-Carmona, P.; Halik, Ü.; Sawut, M.; Caetano, M. Effects of green space spatial pattern on land surface temperature: Implications for sustainable urban planning and climate change adaptation. *ISPRS J. Photogramm. Remote Sens.* **2014**, *89*, 59–66. [CrossRef]
21. Benz, S.; Bayer, P.; Göttsche, F.-M.; Olesen, F.; Blum, P. Linking Surface Urban Heat Islands with Groundwater Temperatures. *Environ. Sci. Technol.* **2015**, *50*, 70–78. [CrossRef] [PubMed]
22. Dědeček, P.; Šafanda, J.; Rajver, D. Detection and quantification of local anthropogenic and regional climatic transient signals in temperature logs from Czechia and Slovenia. *Clim. Chang.* **2012**, *113*, 787–801. [CrossRef]
23. Hemmerle, H.; Bayer, P. Climate Change Yields Groundwater Warming in Bavaria, Germany. *Front. Earth Sci.* **2020**, *8*. [CrossRef]
24. Strauch, G.; Möder, M.; Wennrich, R.; Osenbrück, K.; Gläser, H.-R.; Schladitz, T.; Müller, C.; Schirmer, K.; Reinstorf, F.; Schirmer, M. Indicators for assessing anthropogenic impact on urban surface and groundwater. *J. Soils Sediments* **2008**, *8*, 23–33. [CrossRef]
25. Hähnlein, S.; Bayer, P.; Ferguson, G.; Blum, P. Sustainability and policy for the thermal use of shallow geothermal energy. *Energy Policy* **2013**, *59*, 914–925. [CrossRef]

26. Jesußek, A.; Köber, R.; Grandel, S.; Dahmke, A. Aquifer heat storage: Sulphate reduction with acetate at increased temperatures. *Environ. Earth Sci.* **2013**, *69*, 1763–1771. [CrossRef]

27. Kløve, B.; Ala-Aho, P.; Bertrand, G.; Gurdak, J.J.; Kupfersberger, H.; Kværner, J.; Muotka, T.; Mykrä, H.; Preda, E.; Rossi, P.; et al. Climate change impacts on groundwater and dependent ecosystems. *J. Hydrol.* **2014**, *518*, 250–266. [CrossRef]

28. Saito, T.; Hamamoto, S.; Ueki, T.; Ohkubo, S.; Moldrup, P.; Kawamoto, K.; Komatsu, T. Temperature change affected groundwater quality in a confined marine aquifer during long-term heating and cooling. *Water Res.* **2016**, *94*, 120–127. [CrossRef]

29. Vienken, T.; Händel, F.; Epting, J.; Dietrich, P.; Liedl, R.; Huggenberger, P. Energiewende braucht Wärmewende—Chancen und Limitierungen der intensiven thermischen Nutzung des oberflächennahen Untergrundes in urbanen Gebieten vor dem Hintergrund der aktuellen Energiedebatte in Deutschland. *Grundwasser* **2016**, *21*, 69–73. [CrossRef]

30. Barla, M.; Di Donna, A. Energy tunnels: Concept and design aspects. *Undergr. Space* **2018**, *3*, 268–276. [CrossRef]

31. Baralis, M.; Barla, M.; Bogusz, W.; Di Donna, A.; Ryżyński, G.; Żeruń, M. Geothermal Potential of the NE Extension Warsaw Metro Tunnels. *Environ. Geotech.* **2018**, 1–37. [CrossRef]

32. Yoshitake, I.; Yasumura, N.; Syobuzako, M.; Scanlon, A. Pipe Heating System with Underground Water Tank for Snow Thawing and Ice Prevention on Roads and Bridge Decks. *J. Cold Reg. Eng.* **2011**, *2*, 71–86. [CrossRef]

33. Baumgärtel, S.; Rohn, J.; Luo, J. Experimental study of road deicing by using the urban groundwater under the climatic condition of Nuremberg city, Germany. *SN Appl. Sci.* **2020**, *2*, 537. [CrossRef]

34. Zhu, K.; Blum, P.; Ferguson, G.; Balke, K.-D.; Bayer, P. The geothermal potential of urban heat islands. *Environ. Res. Lett.* **2011**, *6*, 019501. [CrossRef]

35. Arola, T.; Korkka-Niemi, K. The effect of urban heat islands on geothermal potential: Examples from Quaternary aquifers in Finland. *Hydrogeol. J.* **2014**, *22*, 1953–1967. [CrossRef]

36. Zhang, Y.; Soga, K.; Choudhary, R. Shallow geothermal energy application with GSHPs at city scale: Study on the City of Westminster. *Géotech. Lett.* **2014**, *4*, 125–131. [CrossRef]

37. Kłonowski, M.; Herms, I.; Goetzl, G.; Borović, S.; Garcia-Gil, A.; Ditlefsen, C.; Boon, D.; Veloso, F.M.L.; Petitclerc, E.; Janža, M.; et al. Managing Urban Shallow Geothermal Energy (Preliminary Results of the MUSE Project). In *Proceedings World Geothermal Congress*; Reykjavik, Iceland, 2020; Available online: https://www.researchgate.net/publication/337623397_Managing_Urban_Shallow_Geothermal_Energy_Preliminary_Results_of_the_MUSE_Project (accessed on 4 January 2021).

38. Geo-net, U.G. *Stadtklimagutachten—Analyse der klimaökologische Funktionen für das Stadtgebiet von Nürnberg*; GEO-NET Umweltconsulting GmbH: Hannover, Germany, 2014; p. 131.

39. Berger, K. *Erläuterungen zur Geologischen Karte Nürnberg-Fürth-Erlangen und Umgebung 1:50,000*; Bayerisches Geologisches Landesamt: Munich, Germany, 1978; p. 219.

40. Fuchs, B. *Erläuterungen zur Geologischen Karte von Bayern, 1:250,000, Blatt Nr-6532 Nürnberg*; Bayerisches Geologisches Landesamt: Munich, Germany, 1956.

41. Lawa, L.W. *Grundwasser—Richtlinien für Beabachtung und Auswertung, Teil 2 Grundwassertemperatur*; Woeste Druck + Verlag: Essen, Germany, 1987; p. 34.

42. Luo, J. *Experimental Measurements and Numerical Modeling of a Ground Source Heat Pump System*; Friedrich-Alexander-Universität Erlangen-Nürnberg: Erlangen, Germany, 2014.

43. de Wall, H.; Schaarschmidt, A.; Kämmlein, M.; Gabriel, G.; Bestmann, M.; Scharfenberg, L. Subsurface granites in the Franconian Basin as the source of enhanced geothermal gradients: A key study from gravity and thermal modeling of the Bayreuth Granite. *Int. J. Earth Sci.* **2019**, *108*, 1913–1936. [CrossRef]

44. VDI 4640/1. VDI 4640 Blatt 1: 2010-06: Thermal use of the underground. In *VDI-Gesellschaft Energie und Umwelt*; VDI-Gesellschaft Energie und Umwelt: Düsseldorf, Germany, 2010; p. 33.

45. Makinde, E.O.; Agbor, C.F. Geoinformatic assessment of urban heat island and land use/cover processes: A case study from Akure. *Environ. Earth Sci.* **2019**, *78*, 483. [CrossRef]

46. Zhu, K.; Bayer, P.; Grathwohl, P.; Blum, P. Groundwater temperature evolution in the subsurface urban heat island of Cologne, Germany. *Hydrol. Process.* **2014**, *29*, 965–978. [CrossRef]

47. Baier, A.; van Geldern, R.; Löhr, G.; Subert, H.L.; Barth, J.A.C. Grundwasser in Nürnberg: Wichtige Einheiten und deren Nutzbarkeit. *Grundwasser* **2016**, *21*, 253–266. [CrossRef]

48. Löhr, G. *Hydrogeologie. Grundwasserbericht 2011. Daten zur Nürnberger Umwelt*; Stadt Nürnberg/Umweltreferat: Nürnberg, Germany, 2011; pp. 27–32.

49. Hemmerle, H.; Hale, S.; Dressel, I.; Benz, S.; Attard, G.; Blum, P.; Bayer, P. Estimation of Groundwater Temperatures in Paris, France. *Geofluids* **2019**, *2019*, 1–11. [CrossRef]